Journal of Computational Physics **178,** 58–80 (2002)
doi:10.1006/jcph.2002.7018, available online at http://www.idealibrary.com on IDEAL®

A Two-Scale Method for the Computation of Solid–Liquid Phase Transitions with Dendritic Microstructure

Christof Eck, Peter Knabner, and Sergey Korotov

Institute for Applied Mathematics, University of Erlangen—Nürnberg, Erlangen D-91058, Germany
E-mail: eck@am.uni-erlangen.de

Received March 28, 2001; revised January 25, 2002

A two-scale model for liquid–solid phase transitions with equiaxed dendritic microstructure in binary material in the case of slow solute diffusion is presented. The model consists of a macroscopic energy transport equation and, for each point of the macroscopic domain, a local cell problem describing the evolution of the microstructure and the microsegregation. It is derived by formal homogenization of a sharp interface model, including the Gibbs–Thomson law and kinetic undercooling. Based on the two-scale model, a numerical two-scale method for the simulation of phase transitions with dendritic microstructure is developed, and numerical examples are presented.

Key Words: Stefan problem; Gibbs–Thomson law; kinetic undercooling; homogenization; multiscale model; crystal growth.

1. INTRODUCTION

In liquid–solid phase transitions such as the casting of metals often a specific dendritic microstructure of the phase interface is observed. In Fig. 1, on the right half, the *equiaxed* morphology is depicted; it consists of crystals starting to grow from small initial seeds in all directions. On the left side the columnar growth is shown, consisting of columnar dendrites growing in the direction of the heat flow. In both cases a side branching into dendritic arms of second or sometimes even third order is observed. The microstructure has a profound influence on the properties and the quality of the material. It affects in particular the grain structure and the microsegregation (small-scale variations of the composition of the material). The microstructure is the consequence of an instability of a "flat" liquid–solid interface with respect to small perturbations. It scale must be limited by surface energy terms. The phenomenologically simplest models capable of describing the evolution of microstructure on the microscopic scale are sharp interface models with surface tension given

0021-9991/02 $35.00

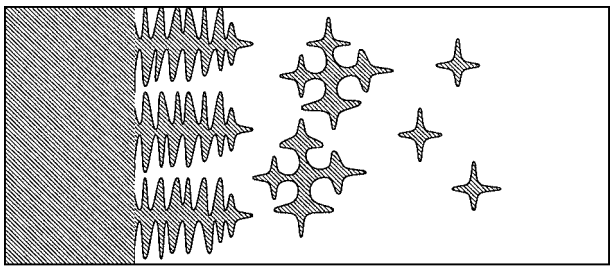

FIG. 1. Microstructure in liquid–solid phase transitions.

by the Gibbs–Thomson law and possibly kinetic undercooling. The numerical simulation of single-crystal growth is a well-studied task; numerical techniques range from interface-tracking methods [2, 10, 21, 22], to level-set methods [24], to phase-field methods [4, 12, 28]. However, these methods need a very detailed resolution of every crystal in order to give reliable results; therefore they are not directly applicable to the simulation of a whole macroscopic structure such as a cast. In the past decade there has been considerable effort put into developing purely macroscopic models for the microstructure evolution in castings (see, e.g., [3, 23]). However, these models usually need evolution laws for certain parameters of the microstructure which can be derived only in the case of very simple model problems with a limited range of validity.

In this contribution a new two-scale model for the evolution of an equiaxed microstructure in binary material with "fast" heat and "slow" solute diffusion is presented. The model is based on a decomposition of the process into two scales, with the macroscopic scale having the size of the whole domain and the microscopic scale that of single crystals. This is done by coupling a macroscopic homogenized energy transport equation with microscopic cell problems describing the evolution of the single crystals and the microsegregation. The model is derived by homogenization via formal asymptotic expansion of a sharp interface model for binary material involving surface energy and kinetic undercooling. The sharp interface model is presented in Section 2. In Section 3 the formal homogenization is carried out and the two-scale model is presented. In Section 4 the discretization of the two-scale model by finite elements and the solution methods for the microscopic cell problems are explained. Section 5 contains the results of numerical computations in two space dimensions.

2. THE SHARP INTERFACE MODEL

In a sharp interface model (Fig. 2) the domain under consideration, $\Omega \subset \mathbb{R}^N$ with space dimension $N \in \mathbb{N}$, is separated at each time $t \in I_{\mathcal{T}}$ with time interval $I_{\mathcal{T}} = [0; \mathcal{T}]$ into a domain $\Omega_\ell(t)$ containing only liquid material and $\Omega_s(t)$ containing the solidified material. Both domains are separated by the phase interface $\Gamma_I(t)$. These domains vary in time, and they are a priori unknown; their determination is part of the problem. The required variables in a phase-transition problem for binary material are temperature T, concentration c_k of one of the components of the material in liquid ($k = \ell$) and solid ($k = s$) material, and velocity v_s of the phase interface, measured in the direction of the outer normal n_s of the solid domain. The material properties shall be described by the density of internal energy $u_k = u_k(T, c_k)$, $k = \ell, s$, the chemical potential $\mu_k = \mu_k(T, c_k)$, the heat conductivity $K^{(k)}$, the solute diffusivity $D^{(k)}$, the curvature multiplier σ, the kinetic multiplier β, and a function

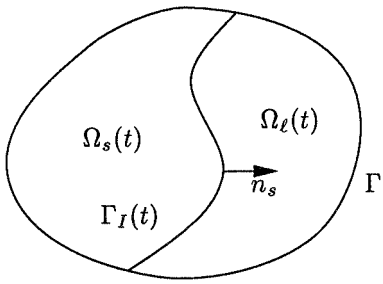

FIG. 2. Sharp interface model.

$b(T, \mu)$ derived from the phase diagram. Then the model studied here is given by the differential equations

$$\partial_t u_k - \nabla \cdot \left(K^{(k)} \nabla T\right) - \nabla \cdot \left(D^{(k)} \frac{\partial u_k}{\partial c_k} \nabla c_k\right) = f, \tag{1}$$

$$\partial_t c_k - \nabla \cdot \left(D^{(k)} \nabla c_k\right) = 0, \tag{2}$$

defined for $t \in I_{\mathcal{T}}$ and $x \in \Omega_k(t)$, $k = \ell, s$; by the boundary conditions on the phase interface $\Gamma_I(t)$,

$$\mu_\ell(T, c_\ell) = \mu_s(T, c_s), \tag{3}$$

$$\left[K \frac{\partial T}{\partial n} + D \frac{\partial u}{\partial c} \frac{\partial c}{\partial n}\right] = -[u] v_s, \tag{4}$$

$$\left[D \frac{\partial c}{\partial n}\right] = -[c] v_s, \tag{5}$$

$$b(T, \mu) = -\sigma\kappa - \beta v_s; \tag{6}$$

by boundary conditions on the boundary of the whole domain $\Gamma = \partial\Omega$,

$$K \frac{\partial T}{\partial n} + \alpha T = f_\Gamma, \tag{7}$$

$$D \frac{\partial c}{\partial n} = 0; \tag{8}$$

and by initial conditions

$$T(t = 0, x) = T^{(0)}(x) \quad \text{and} \quad c(t = 0, x) = c^{(0)}(x), \quad x \in \Omega,$$

for temperature and concentration and by

$$\Omega_s(t = 0) = \Omega_s^{(0)}$$

for the initial partition into solid and liquid domain. The function f in (1) represents a volume heat source, and the coefficient α and the function f_Γ in (7) describe a heat exchange condition at the boundary with heat exchange coefficient α and outer temperature $\frac{f_\Gamma}{\alpha}$. The letter κ denotes the mean curvature, taken positive for Ω_s being convex, and

the bracket $[\cdot]$ denotes the jump of the corresponding quantity at the phase interface, more precisely, $[K\frac{\partial T}{\partial n}] := K^{(\ell)}\nabla T_\ell \cdot n_\ell + K^{(s)}\nabla T_s \cdot n_s$ and $[u] := u_s - u_\ell$. The functions u_k and μ_k are assumed to be sufficiently smooth, but they may be different in solid and liquid. Equation (1) is a heat transport equation, where the second term corresponds to energy transport due to heat diffusion and the third one to energy transport due to solute diffusion; Eq. (2) is a standard solute diffusion equation. Condition (3) prescribes continuity of the chemical potential across the interface; since the functions μ_s and μ_ℓ are usually not equal, this implies a discontinuity of the concentration, the *miscibility gap*. Conditions (4) and (5) are local conservation laws for energy and solute across the interface Γ_I moving with velocity v_s in the direction of the outward normal of Ω_s. Equation (6) is a generalized Stefan condition with Gibbs–Thomson undercooling and kinetic undercooling adapted to the case of a binary mixture. This condition determines the velocity v_s of the interface Γ_I. The function b is specified from the physics of the phase transition, in particular from the phase diagram. In the simplest case of a linear model it is given by $b(T, \mu) = b_1 T + b_2\mu + b_3$ with constants b_1, b_2, and b_3.

The model described here is studied in [15] for the case of vanishing kinetic coefficient $\beta = 0$. There, the function $b(T, \mu)$ is taken as the solid–liquid difference $b(T, \mu) = [g(T, \mu)] := g_s(T, \mu) - g_\ell(T, \mu)$ of the Legendre transform $g_k := \frac{u_k}{T} - \frac{\mu_k}{T}c_k - s_k$ of the entropy s_k with respect to the variables $\frac{1}{T}$ and $-\frac{\mu}{T}$. The existence of a weak solution is proved under some growth conditions for the entropy. In this case, however, the solution is not unique in general. Existence and uniqueness results for vanishing kinetic coefficients have been proved only recently for pure material [1, 7]. For the case of nonvanishing kinetic coefficients (whose mathematical structure is simpler), also only the case of pure material has been studied. Existence and uniqueness results are derived in [6, 19].

3. HOMOGENIZATION AND TWO-SCALE MODEL

In this section we consider an idealized microstructure consisting of equiaxed crystals whose midpoints are located at the sites of a uniform grid, c.f., Fig. 3. The scale of the microstructure is given by a small parameter, $\varepsilon > 0$, signifying the spacing of this grid. This situation may arise in the case of *instantaneous* nucleation, where small solid kernels of a given distribution and a given size nucleate at a given undercooling. The assumption of periodic distribution of the initial kernels is, of course, not very realistic, but it is frequently made in homogenization theory in order to derive macroscopic models which are then also used for more general situations. The initial conditions of the problem have to reflect this instantaneous periodic nucleation; more precisely we assume initial temperature and

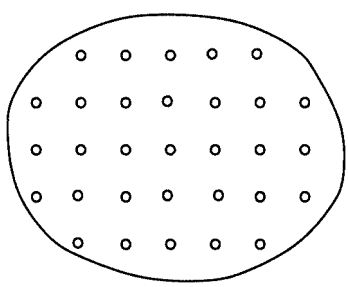

FIG. 3. Idealized initial microstructure.

concentration to be given by

$$T_\varepsilon(t=0,x) = T^{(0)}\left(x, \frac{x}{\varepsilon}\right), \tag{9}$$

$$c_\varepsilon(t=0,x) = c^{(0)}\left(x, \frac{x}{\varepsilon}\right), \tag{10}$$

with functions $T^{(0)}, c^{(0)} \in C^1(\Omega, L_{2\#}(Y))$, where $Y \subset \mathbb{R}^N$ is a periodicity cell and $L_{2\#}(Y) := \{y \in L_2(\mathbb{R}^N) \mid y \text{ is } Y\text{-periodic}\}$, and an initial solid domain given by

$$\Omega_s^{(0)} := \Omega \cap \bigcup_{k\in\mathbb{Z}^N} \varepsilon\left(\{k\} \oplus Y_s^{(0)}\right)$$

with unit solid domain $Y_s^{(0)} \subset Y$. Here, T_ε and c_ε denote solutions of the problem with scale parameter ε; in fact we consider a whole family of problems depending on parameter ε.

In homogenization theory it is often necessary to scale several physical parameters of the problem, too. In order to maintain an equilibrium between surface and volume energy, the density of surface energy σ is scaled proportional to ε,

$$\sigma = \varepsilon\sigma_0.$$

The solute diffusivity is scaled proportional to ε^2,

$$D^{(k)} = \varepsilon^2 D_0^{(k)};$$

this is justified by the fact that solute diffusivity is usually much smaller than heat conductivity. It is moreover known from material sciences that solute diffusivity is one of the parameters determining the scale of the microstructure. The kinetic coefficient is scaled proportional to ε^{-1},

$$\beta = \varepsilon^{-1}\beta_0.$$

Finally, let us remark that the curvature κ of a surface which is scaled by a factor ε is proportional to ε^{-1}, $\kappa = \kappa_0\varepsilon^{-1}$.

The homogenization will be carried out by the method of asymptotic expansions. It is assumed that the functions T_ε and c_ε and the velocity v_ε of the phase interface admit the asymptotic representations

$$\begin{aligned}
T_\varepsilon(t,x) &= T_0\left(t,x,\frac{x}{\varepsilon}\right) + \varepsilon T_1\left(t,x,\frac{x}{\varepsilon}\right) + \varepsilon^2 T_2\left(t,x,\frac{x}{\varepsilon}\right) + \cdots,\\
c_\varepsilon(t,x) &= c_0\left(t,x,\frac{x}{\varepsilon}\right) + \varepsilon c_1\left(t,x,\frac{x}{\varepsilon}\right) + \varepsilon^2 c_2\left(t,x,\frac{x}{\varepsilon}\right) + \cdots,\\
v_\varepsilon(t,x) &= \varepsilon v_0\left(t,x,\frac{x}{\varepsilon}\right) + \varepsilon^2 v_1\left(t,x,\frac{x}{\varepsilon}\right) + \cdots
\end{aligned} \tag{11}$$

valid for small ε. The leading orders T_0, c_0, and v_0 of these functions are given by the limit $\varepsilon \to 0$. In order to compute these limits, the asymptotic expansions (11) are plugged into problem (1)–(8), and the coefficients of different orders of ε are collected, starting from the lowest order. The gradient of a function $f(x, \frac{x}{\varepsilon})$ depending on a "slow" variable x and a

"fast" variable $y = \frac{x}{\varepsilon}$ is given by $\nabla f = \nabla_x f + \frac{1}{\varepsilon}\nabla_y f_{|y=\frac{x}{\epsilon}}$ or, shortly, $\nabla = \nabla_x + \frac{1}{\varepsilon}\nabla_y$. This leads to a sequence of problems of different orders.

The *problem of 0th order* consists of the terms in Eq. (1) of order ε^{-2}, of the continuity of the temperature of order ε^0, and of Eq. (4) of order ε^{-1},

$$\begin{aligned} -\nabla_y \cdot \left(K^{(k)} \nabla_y T_0\right) &= 0 \quad \text{in } Y_k(t,x),\ k = \ell, s, \\ [K \nabla_y T_0 \cdot n_y] &= 0 \quad \text{on } \Gamma_I(t,x), \\ [T_0] &= 0 \quad \text{on } \Gamma_I(t,x), \end{aligned}$$

and T_0 satisfies periodic boundary conditions on ∂Y. Here, Y_k for $k = \ell$ and $k = s$ denote the liquid and solid part of the unit cell Y, and n_y is the unit normal vector on their common boundary Γ_I, pointing outward from Y_s. The solutions of the problem of 0th order are constant functions. Hence, T_0 is independent of y, $T_0 = T_0(t,x)$.

The *problem of 1st order* consists of the terms in Eq. (1) of order ε^{-1}, of the continuity of the temperature of order ε^1, and of Eq. (4) of order ε^0,

$$\begin{aligned} -\nabla_y \cdot \left(K^{(k)}(\nabla_y T_1 + \nabla_x T_0)\right) &= 0 \quad \text{in } Y_k(t,x),\ k = \ell, s, \\ [K(\nabla_y T_1 + \nabla_x T_0) \cdot n_y] &= 0 \quad \text{on } \Gamma_I(t,x), \\ [T_1] &= 0 \quad \text{on } \Gamma_I(t,x), \end{aligned}$$

and T_1 satisfies periodic boundary conditions on ∂Y. Observe that the term $\nabla_y T_0$ vanishes. This is again a standard elliptic boundary value problem in variable y with a right hand side depending on the constant vector $\nabla_x \cdot T_0(t,x)$. Since the problem is linear, the solution can be represented by

$$T_1(t,x,y) = \sum_{j=1}^{N} H_j(t,x,y)\partial_{x_j} T_0(t,x), \tag{12}$$

where H_j, $j = 1, \ldots, N$, are solutions of the *local cell problems*

$$\begin{aligned} -\nabla_y \cdot \left(K^{(k)} \nabla_y H_j\right) &= \nabla_y \cdot \left(K^{(k)} e_j\right) \quad \text{in } Y_k(t,x),\ k = \ell, s, \\ [K \nabla_y H_j \cdot n_y] &= -[K e_j \cdot n_y] \quad \text{on } \Gamma_I(t,x) \end{aligned} \tag{13}$$

satisfying periodic boundary conditions on ∂Y. Here, e_j denotes the jth unit vector in $\mathbb{R}^N$. If the heat conductivity is constant and its value in the liquid and the solid is equal, $K^{(\ell)} = K^{(s)}$, then the term $T_1(t,x,y)$ is also independent of y.

The *problem of 2nd order* consists of the order ε^0 terms in (1)–(3) and (6), the order ε^1 terms in (4) and (5), and the order ε^2 terms in the continuity of the temperature,

$$\begin{aligned} &\partial_t u_k\left(T_0, c_0^{(k)}\right) - \nabla_y \cdot \left(K^{(k)} \nabla_y T_2\right) - \nabla_x \cdot \left(K^{(k)}(\nabla_x T_0 + \nabla_y T_1)\right) \\ &\quad -\nabla_y \cdot \left(K^{(k)} \nabla_x T_1 + D_0^{(k)} \frac{\partial u_k}{\partial c_k} \nabla_y c_0^{(k)}\right) = f \quad \text{in } \Omega \times Y_k(t), \end{aligned} \tag{14}$$

$$\left[\left(K(\nabla_y T_2 + \nabla_x T_1) + D_0 \frac{\partial u}{\partial c} \nabla_y c_0\right) \cdot n_y\right] + [u(T_0, c_0)] v_0 = 0 \quad \text{on } \Omega \times \Gamma_I(t), \tag{15}$$

$$\partial_t c_0^{(k)} - \nabla_y \cdot \left(D_0^{(k)} \nabla_y c_0^{(k)}\right) = 0 \quad \text{in } \Omega \times Y_k(t), \tag{16}$$

$$\mu_\ell\left(T_0, c_0^{(\ell)}\right) = \mu_s\left(T_0, c_0^{(s)}\right) \quad \text{on } \Omega \times \Gamma_I(t), \tag{17}$$

$$[D_0 \nabla_y c_0 \cdot n_y] + [c_0] v_0 = 0 \quad \text{on } \Omega \times \Gamma_I(t), \tag{18}$$

$$b(T_0, \mu_0) = -\sigma_0 \kappa_0 - \beta_0 v_0 \quad \text{on } \Omega \times \Gamma_I(t). \tag{19}$$

We integrate Eq. (14) with respect to $y \in Y$ and use the Green theorem for the $\nabla_y \cdot$ terms and the exchange relation $\partial_t \int_{Y_s(t)} w(t, y)\, dy = \int_{Y_s(t)} \partial_t w(t, y)\, dy + \int_{\partial Y_s(t)} w(t, y) v_s(t, y)\, ds_y$ with the interface velocity v_s. Then, from relation (15) it is seen that the boundary terms at the phase interface vanish, and those at the boundary ∂Y of the unit cell vanish due to the periodic boundary condition. Thus the *macroscopic heat transport equation*

$$\partial_t u^*_{c_0, Y_s}(T_0) - \nabla \cdot (K^* \nabla T_0) = f \quad \text{in } \Omega \tag{20}$$

is obtained, with the averaged density of internal energy

$$u^*_{c_0, Y_s}(T_0) = \sum_{k=\ell,s} \int_{Y_k} u_k\left(T_0, c_0^{(k)}\right) dy,$$

the effective heat conductivity

$$K^*_{ij} = \sum_{k=\ell,s} \int_{Y_k} \left(K_{ij}^{(k)} + \sum_{r=1}^{N} K_{ir}^{(k)} \partial_{y_r} H_j \right) dy, \tag{21}$$

and a possibly averaged heat source f. Equations (16)–(19) represent a family of generalized Stefan problems for concentration c_0 and the partition into solid domain Y_s and liquid domain Y_ℓ, depending on the parameter $x \in \Omega$ and on the local macroscopic temperature evolution $T(\cdot, x)$ as given data. They can be interpreted as *local cell problems* for the microsegregation c_0 and the evolution of the dendritic microstructure,

$$\partial_t c_k(T_0; \mu_0) - \nabla_y \cdot \left(\tilde{D}_0^{(k)} \nabla_y \mu_0\right) = 0 \quad \text{in } Y_k(t), k = \ell, s, \tag{22}$$

$$[\tilde{D}_0 \nabla_y \mu_0 \cdot n_y] + [c(T_0; \mu_0)] v_0 = 0 \quad \text{on } \Gamma_I(t), \tag{23}$$

$$b(T_0, \mu_0) = -\sigma_0 \kappa_0 - \beta_0 v_0 \quad \text{on } \Gamma_I(t). \tag{24}$$

Here, in order to illustrate the structure as a generalized Stefan problem, the chemical potential μ is used as variable. This requires a modification of the diffusivity to $\tilde{D}^{(k)} = D^{(k)} \frac{\partial c_k}{\partial \mu}$.

The result of the formal homogenization is a two-scale model, consisting of a macroscopic energy transport equation for the temperature T—which is constant on the microscopic scale—and, at each point x of the macroscopic domain, a local cell problem describing the evolution of the microstructure and the local variation of the concentration. Both problems are coupled, with the internal energy and the heat conductivity of the macroscopic problem depending on the variation of the concentration and on solid and liquid domains in the microscopic problem; and the function $b(T, \mu)$ determining the equilibrium melting point for μ depends on the macroscopic temperature.

4. NUMERICAL METHOD

In order to illustrate the application of the two-scale model in a numerical algorithm, we consider the simplest case, with constant diffusivity tensors independent of the phases, with linear internal energy $u_k(T, c) = c_V T + \delta_{k\ell} L$ independent of the concentration, and with chemical potential $\mu = \mu_k(c_k) = c_k + \delta_{k\ell}\lambda$, with constant miscibility gap λ and linear function $b(T, \mu) = b_1 T + b_2 \mu$. In this case, the effective heat conductivity is equal to the constant original one, $K^* = K$. This leads to a problem consisting of the macroscopic heat transport equation

$$\begin{aligned} \partial_t(c_V T - \varepsilon_s L) - \nabla \cdot (K \nabla T) &= f \quad \text{in } \Omega, \\ K \frac{\partial T}{\partial n} &= f_\Gamma \quad \text{on } \Gamma, \end{aligned} \tag{25}$$

with solid volume fraction $\varepsilon_s(t, x) = \frac{|Y_s(t,x)|}{|Y|}$ and microscopic cell problem

$$\begin{aligned} \partial_t \mu - \nabla_y \cdot (D \nabla_y \mu) &= 0 \quad \text{in } Y_k(t),\ k = \ell, s, \\ \left[D \frac{\partial \mu}{\partial n_y} \right] + \lambda v_s &= 0 \quad \text{on } \Gamma_I(t), \\ b_1 T + b_2 \mu &= -\sigma\kappa - \beta v_s \quad \text{on } \Gamma_I(t). \end{aligned} \tag{26}$$

Both problems are still coupled; the release of latent heat in the macroscopic problem depends on the microscopic solid volume fraction, and the equilibrium melting point in the microscopic problem depends on the macroscopic temperature.

Let us comment on the thermodynamical consistency of such a model. For an internal energy of the form $u_k = c_V T + \delta_{k\ell} L$, the corresponding entropy is given by $s = s_k = c_V \ln(T) - a_k(c_k)$ with suitable functions a_k, $k = \ell, s$, and the chemical potential is $\mu = \mu_k(T, c_k) = a_k'(c_k) T$. The Legendre transform $s_k^* = \frac{1}{T} u_k - \frac{\mu}{T} c_k - s_k$ is then given by $s_k^* = c_V(1 - \ln(T)) + \delta_{k\ell} \frac{L}{T} - \frac{\mu}{T} c_k + a_k(c_k)$ and from this it follows that its solid–liquid difference $b(T, \mu) = [s^*(T, \mu)]$ is not linear. Therefore the completely linear model given above is, in general, not thermodynamically consistent. It can be interpreted as a linearization of a thermodynamically consistent model; e.g., for the special choice $a_k(c_k) = \frac{1}{2}(c_k + \delta_{k\ell}\lambda)^2$ we have $\mu_k(T, c_k) = (c_k + \delta_{k\ell}\lambda) T$ and $b(T, \mu) = -\frac{L}{T} - \lambda \frac{\mu}{T}$. Linearization of μ_k and b around some point (T_0, μ_0) with corresponding concentrations c_{k0}, $k = \ell, s$, gives $\mu_k = (T - T_0)(c_{k0} + \delta_{k\ell}\lambda) + T_0(c_k - c_{k0})$ and $b(T, \mu) = \frac{L + \lambda\mu_0}{T_0^2}(T - T_0) - \frac{\lambda}{T_0}(\mu - \mu_0)$. Hence, up to an additive constant the linear model given above is obtained.

The model can be also interpreted as a thermodynamically consistent linear one, but in this case the interpretation of variables is changed. Let $\tilde{T} = -\frac{1}{T}$ and $\tilde{\mu} = \frac{\mu}{T}$ denote the "dual" variables to internal energy and concentration and let us assume the linear constitutive law $u_k = \tilde{T} + \delta_{k\ell} L$ for internal energy and $c_k = \tilde{\mu} - \delta_{k\ell}\lambda$ for the relation between chemical potential and concentration. Then the entropy satisfies the relations $ds = -\tilde{T}\, du - \tilde{\mu}\, dc$ and can be defined as $s = -\frac{1}{2}(\tilde{T}^2 + \tilde{\mu}^2)$ in both solid and liquid material. Its Legendre transform is $s_k^* = -\tilde{T} u_k - \tilde{\mu} c_k - s_k = -\frac{1}{2}(\tilde{T}(\tilde{T} + 2L\delta_{k\ell}) + \tilde{\mu}(\tilde{\mu} - 2\lambda\delta_{k\ell}))$ in solid ($k = s$) and liquid ($k = \ell$) material; consequently the solid–liquid difference is $[s^*(\tilde{T}, \tilde{\mu})] = \tilde{T} L - \tilde{\mu}\lambda$. With this new interpretation of variables the linear model is thermodynamically consistent.

4.1. Discretization

Both the macroscopic heat transport equation (25) and the microscopic diffusion equation (26) are discretized by finite differences in the time variable and finite elements in the space variables. Let $T_h^{(\ell)}$ denote the coefficient vector of a representation of the discrete (macroscopic) temperature at time step ℓ with respect to a corresponding finite-element basis of a subspace of $H^1(\Omega)$. Then we have a sequence of linear equations for the temperature $T_h^{(\ell)}$,

$$(c_V M_{\Omega h} + \Theta \Delta t K_{\Omega h}) T_h^{(\ell)} = R_{\Omega h} + L M_{\Omega h} \varepsilon_{sh}^{(\ell)}, \tag{27}$$

with mass matrix $M_{\Omega h}$, stiffness matrix $K_{\Omega h}$, and $\varepsilon_{sh}^{(\ell)}$ denoting the discretization of the solid volume fraction computed from the microscopic problem. The right hand side $R_{\Omega h}$ depends on the temperature $T_h^{(\ell-1)}$ and the solid volume fraction $\varepsilon_{sh}^{(\ell-1)}$ of the preceding time step, on the discretization of the external heat source f and on the time implicity parameter $\Theta \in [0, 1]$. At each nodal point of the macroscopic temperature, a discrete local cell problem is given. If $\mu_h^{(\ell)}$ denotes the coefficient vector of the discrete chemical potential $\mu(t^{(\ell)}, x, \cdot)$ with respect to a finite-element basis of $H^1_{\#}(Y)$, then this problem is given by

$$(M_{Yh} + \Theta \Delta t K_{Yh}) \mu_h^{(\ell)} = R_{Yh} - M_{Yh} P_{Yh} \left(\lambda \chi_{Y_{sh}^{(\ell)}} \right). \tag{28}$$

Here, $\chi_{Y_{sh}^{(\ell)}}$ is the characteristic function of a suitable discretization of the microscopic solid domain $Y_s^{(\ell)}$ at time step ℓ, and P_{Yh} denotes the L_2-projection onto the finite-element space. Equation (28) must be supplemented by an algorithm computing the evolution of the solid phase from some discretized version of the Stefan condition in problem (26). For this task, two different crystal growth algorithms are employed; they are explained in Section 4.2. This also clarifies the definition of $Y_{sh}^{(\ell)}$.

4.2. Algorithms for Crystal Growth

The numerical implementation of the two-scale model for phase transitions in binary material requires the computation of crystal growth for *pure* material (formulated in the chemical potential) on the microscopic scale. There are nowadays several techniques for the computation of crystal growth available. *Front tracking methods* [2, 10, 21, 22] use an explicit representation of the solid–liquid interface and a certain discretization of the generalized Stefan condition; they are often inspired by techniques used to compute mean curvature flow. In *level-set methods* [24] the interface is represented as a line of zeros of an additional function for which a (usually hyperbolic) differential equation is specified. In *phase-field methods* [4, 12, 28] the sharp transition between solid and liquid is approximated by a smooth transition described with a phase field Φ changing continuously from its liquid value (say $\Phi = -1$) to its solid value (e.g., $\Phi = 1$) within a diffuse interface of small thickness. The evolution of the phase field is given by an additional parabolic differential equation. Here, we decided to use and compare two different front-tracking methods: a *variational algorithm* due to Almgren [2], where the Stefan condition is represented as a Euler–Lagrange equation of an optimization problem for the unknown solid domain, and the *method of fully faceted interfaces* due to Roosen and Taylor [21], based on an evolution of a discrete interface represented by a polygonal line having only normals identical to those of the given Wulff shape of the (anisotropic) surface energy. Both methods are shortly described below.

4.2.1. *The Variational Method*

This method will be shortly explained for the case of vanishing kinetic coefficient $\beta = 0$. The Stefan condition in (26) is represented as a Euler–Lagrange equation of the optimization problem

$$Y_s = \text{Arg} \min_{B \in \mathcal{A}} \mathcal{F}_b(B) \tag{29}$$

with functional

$$\mathcal{F}_b(B) := \int_{\partial B} \sigma \, ds_y + \int_B b \, dy,$$

where $b = b(T, \mu)$ here. With $\mathcal{A} \subset \mathcal{P}(Y)$ a set of admissible solid domains is denoted. The appropriate choice of $\mathcal{A}$ is not considered here. The equivalence of problem (29) to the Stefan condition is valid in the following sense: let $B \subset Y$ be a solid domain with smooth boundary ∂B; then a variation B_η of B can be defined via a corresponding variation of the boundary given by a scalar function w defined on ∂B,

$$\partial B_\eta = \{y + \eta w(y) n(y) \mid y \in \partial B\},$$

where n denotes the normal of ∂B pointing outside B (see Fig. 4). Then the variation of $\mathcal{F}$ is given by

$$\langle \delta \mathcal{F}(B), w \rangle := \lim_{\eta \to 0} \frac{1}{\eta} (\mathcal{F}(B_\eta) - \mathcal{F}(B_0)) = \int_{\partial B} [\sigma \kappa + b] w \, ds_y.$$

Hence, the Euler–Lagrange equation $\delta \mathcal{F}(B) = 0$ is equivalent to a weak formulation of the generalized Stefan condition $b = -\sigma \kappa$.

This observation is used in the following way: the solid domain is represented in time step ℓ as the interior of a polygonal curve. The curve is varied by moving its nodal points in certain given directions approximating the normal vectors; this leads to a clearly defined set of admissible discrete solid domains (at least for small variations). Then, for a given function b the optimization problem (29) is finite dimensional and can be solved by standard methods. Here we use a Newton method; if necessary, the Hessian $D^2 \mathcal{F}_{bh}$ of the discretization $\mathcal{F}_{bh}$ of $\mathcal{F}_b$ is changed to a positive definite matrix by adding a certain diagonal matrix, whose entries are computed from a Cholesky decomposition of $D^2 \mathcal{F}_{bh}$. The discrete diffusion

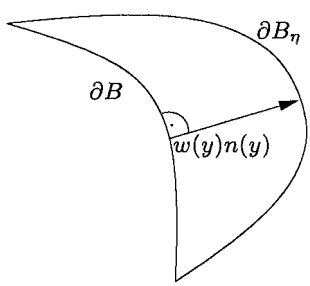

FIG. 4. Variation of a solid domain.

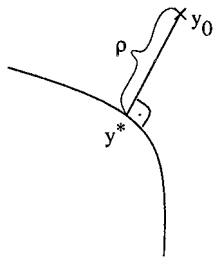

FIG. 5. One-dimensional release of latent heat.

equation (28) and the discrete version of the optimization problem (29) are coupled; in particular we need the chemical potential $\mu^{(\ell)}$ of the current time step for the correct definition of the optimization problem. In order to decouple both problems, the following procedure is employed. First, the diffusion equation is solved with the old solid volume $Y_s^{(\ell-1)}$, this yields a solution μ_A. Then, a corrector term is added which approximately accounts for the temperature change due to release of latent heat. This term may be computed from a one-dimensional heat diffusion problem in normal direction. This is justified, if the interface does not vary very much in the current time step; then the movement of the interface can be locally approximated by a parallel translation of a line and the heat flux due to release of latent heat only has a component perpendicular to this line. Using an approximation with the 1D heat kernel, the correction term can be represented *on the new boundary only* by $\mu_B := \frac{\lambda}{\sqrt{D}} \frac{\rho}{\sqrt{2\pi\,\Delta t}}$, where ρ denotes the distance to the old interface (Fig. 5). This formula is first valid only on the new boundary, which is still unknown. However, it is admissible to replace the functional $\mathcal{F}_{bh}$ by another functional having the same Euler–Lagrange equation in its minimum, since we only compute this minimum. Therefore, the formula can be employed at any point $y \in Y$. This leads to a *precomputed chemical potential* $H := \mu_A + \mu_B$, which is used instead of $\mu^{(\ell)}$ in the optimization problem. Solution of the optimization problem gives the new solid domain $Y_s^{(\ell)}$. Then, the discrete diffusion equation is solved with this new solid domain; this yields the new chemical potential $\mu^{(\ell)}$. For details of the method see [2].

The method has been tested by computing the growth of a single crystal in an undercooled melt. The computation starts from a circular initial seed of radius $r = 0.05$, located at the midpoint of a square with edge length 2.0. The data are specific heat $c_V = 1$, heat conductivity $K = 1$, latent heat $L = 1$, and undercooling $\Delta T = 0.5$. The anisotropic surface tension is given by $\sigma = \sigma_0(1 - \frac{4}{3(m^2-1)}\cos(m\varphi) - \frac{1}{3(4m^2-1)}\cos(2m\varphi))$ with average surface energy $\sigma_0 = 0.001$ and fourfold symmetry $m = 4$. This form of anisotropy is a good approximation of a crystalline anisotropy by means of trigonometric functions. The boundary of the domain is assumed to be isolated. For the space discretization, a uniform rectangular grid with bilinear shape functions is used. Fig. 6 depicts the evolution of the crystal for grid size 400×400 and time step $\Delta t = 0.0001$ up to time 0.1. The driving energy for the solidification is the given undercooling; hence the crystal cannot grow beyond specific solid volume $\varepsilon_s = 0.5$. In Fig. 7, the evolution of specific volume and specific surface is illustrated for grid size 400×400 and various time steps. Figure 8 shows the same data for time step $\Delta t = 0.0001$ and various grid sizes. The considerable differences of these macroscopic values for different discretization parameters clearly indicates that the method only gives reliable results for sufficiently small time steps, and in particular for

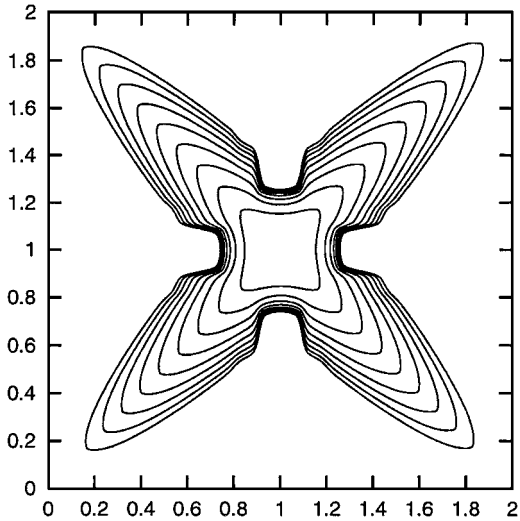

FIG. 6. Variational algorithm. Evolution of crystal up to time 0.1.

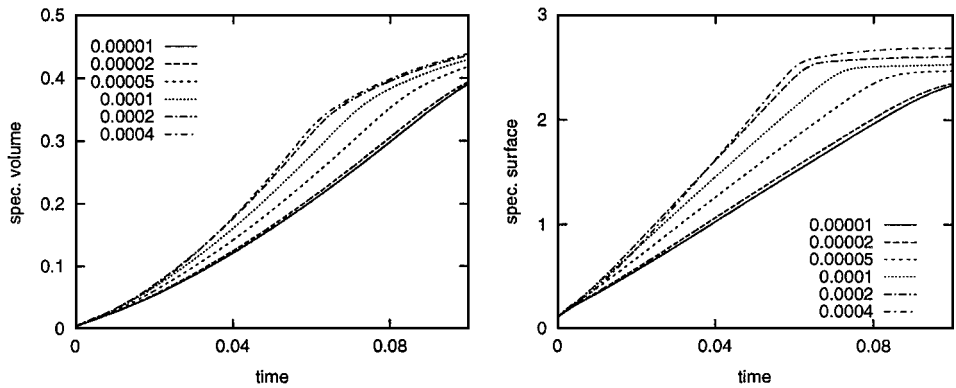

FIG. 7. Variational algorithm. Evolution of specific volume and specific surface for different time steps.

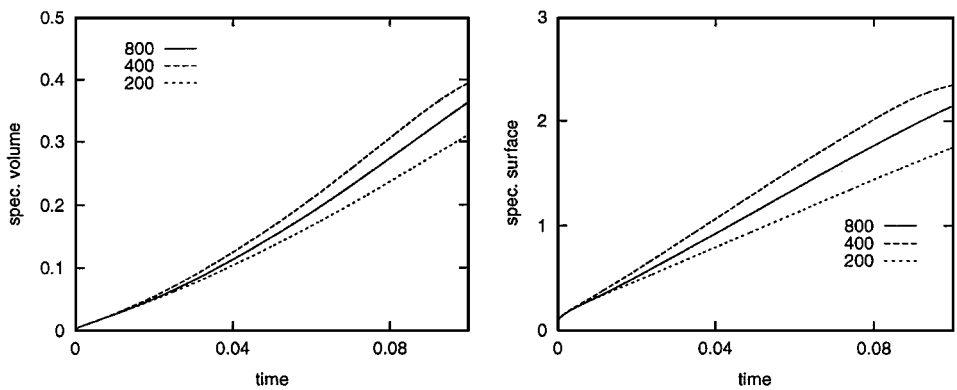

FIG. 8. Variational algorithm. Evolution of specific volume and specific surface for different space discretizations.

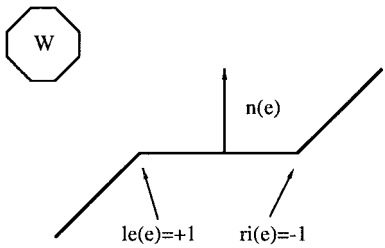

FIG. 9. Crystalline curvature.

sufficiently high grid sizes. This makes the realization of the two-scale method computationally expensive.

4.2.2. *Algorithm of Fully Faceted Interfaces*

The method of fully faceted interfaces is designed for crystalline interfaces in two dimensions, consisting of a polygonal which has only a limited number of admissible normal vectors. As in the previous model, the surface energy may be anisotropic; this is here realized by discrete surface energy densities associated with different admissible normal vectors. Then the *Wulff shape W*, the domain which minimizes the surface energy under the side condition of a given volume, is a convex domain with a polygonal surface (see Fig. 9). An admissible representation of the crystalline surface is given by a polygonal line where two adjacent edges have different normal vectors belonging to two adjacent edges of the Wulff shape. This condition is not as restrictive as it seems; if two adjacent edges have the same normal they can be replaced by one edge, and if they have normal vectors which are not adjacent in the Wulff shape, then we may introduce edges of length zero with corresponding normal vectors in order to connect them.

The method requires a *positive* kinetic coefficient $\beta = M^{-1} > 0$; it is based on the evolution law

$$v_s = -M(b + \sigma\kappa). \tag{30}$$

The mean curvature κ is approximated by a discrete crystalline mean curvature $H(e)$ associated with each element e of the polygonal interface, defined by

$$H(e) = \frac{\mathrm{le}(e) + \mathrm{ri}(e)}{2} \cdot \frac{L(e)}{l(e)}.$$

Here, $\mathrm{le}(e) = 1$ or $\mathrm{le}(e) = -1$ if there is a convex or concave corner at the left end of edge e, $\mathrm{ri}(e)$ has the same definition with respect to the right end of the edge, $l(e)$ denotes the length of edge e, and $L(e)$ is the length of the corresponding edge in the Wulff shape W having the same normal vector (see Fig. 9). This definition of the crystalline curvature already contains the anisotropy of the surface energy; it is included in the length $L(e)$ of the edge in the Wulff shape, but it does not contain the average value $\bar{\sigma}$ of the surface energy. Replacing $\sigma\kappa$ in (30) by $\bar{\sigma}H(e)$ and taking a suitable average $\bar{b}$ of the quantity b over the edge e gives a formula for the rate of advance of edge e. As average $\bar{b}$ we may take the usual integral average $\frac{1}{|e|}\int_e b(x)\,ds_x$ or, alternatively, the value of b at the midpoint of e.

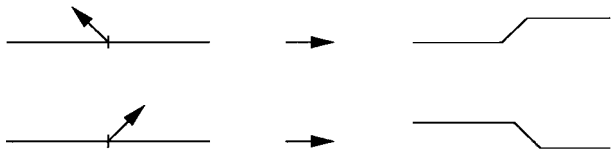

FIG. 10. Shattering of edges.

The equation for the movement of the interface and the diffusion equation are coupled in an explicit way. In each time step $t^{(\ell)}$, first the interface is moved based on the diffusion field $b^{(\ell-1)}$ of the previous time step, then the release of latent heat is calculated, and the diffusion equation is solved. In order to get a good approximation of the crystalline interface, its movement is done by the following steps. First, edges of the interface which are longer than a predefined minimal edge length are shattered into smaller edges (see Fig. 10). Therefore, edges of length zero having different normals than the original edge are introduced. These normals coincide with one of the two adjacent normals corresponding to the respective edge in the Wulff shape. In order to determine the right one of these two normals, one may either use the variation of the diffusion field b along the edge indicating which part will move faster or use a "trial-and-error" procedure. Then, all the edges are moved in the normal direction by a distance prescribed by formula (30). Here, the oriented length of some edges may shrink to zero and then attain negative values; such *flipped* edges are removed, and the two adjacent edges are replaced by a single edge whose location is calculated from the conservation of solid volume (see Fig. 11).

In a continuous time evolution of the crystalline interface it never happens that an edge in a convex or concave part shrinks to zero, because then the crystalline curvature tends to $\pm\infty$. However, in a time discretization this is only true if the time step is suitably adjusted. Therefore, in practice the movement of the interface is done by several adaptively adjusted nested time steps within one step of the time discretization. A more detailed description of the algorithm can be found in [21].

In order to test the method of fully faceted interfaces, the growth of a single crystal in an undercooled melt is computed, starting from an initial seed being a square with edge length $l = 0.1$, which is located at the midpoint of a square with edge length 2.0. The data are specific heat $c_V = 1$, heat conductivity $K = 1$, latent heat $L = 1$, and undercooling $\Delta T = 0.7$; the boundary of the domain is isolated. Observe that the undercooling is slightly bigger than before. The minimal surface tension and velocity multiplier are $\bar{\sigma} = 0.001$ and $\bar{M} = 100$; a spatial anisotropy is induced by multiplication of these values with factors 1 and 1.3 for the diagonal and the horizontal/vertical directions, respectively. The discretization of the heat diffusion equation is the same as that described above. Figure 12 shows the evolution of the crystal for grid spacing 100×100 and time step $\Delta t = 0.0001$ up to time 0.1. In Fig. 13, the evolutions of specific volume and specific surface are illustrated for grid size 100×100 and various time steps. Figure 14 shows the same data for time step $\Delta t = 0.0001$ and various grid spacings. Compared to the variational algorithm, this method gives more stable results even for moderate values of the discretization parameters. The employed kinetic undercooling has a regularizing effect on the problem and simplifies its

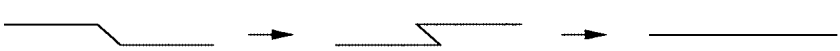

FIG. 11. Removal of flipped edges.

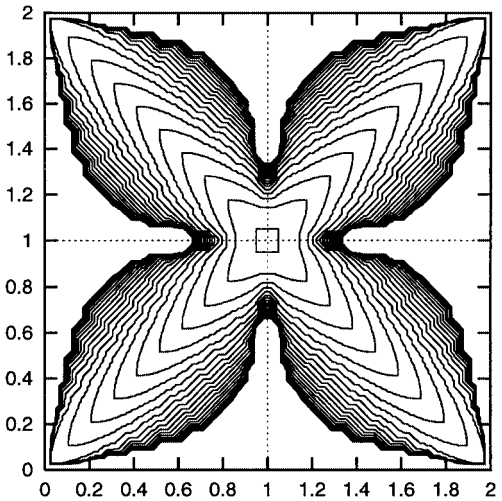

FIG. 12. Method of fully faceted interfaces. Evolution of crystal up to time 0.1.

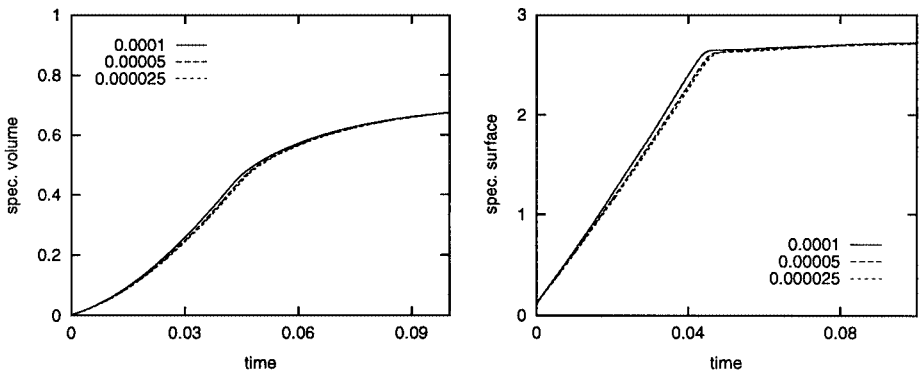

FIG. 13. Method of fully faceted interfaces. Evolution of specific volume and specific surface for different time steps.

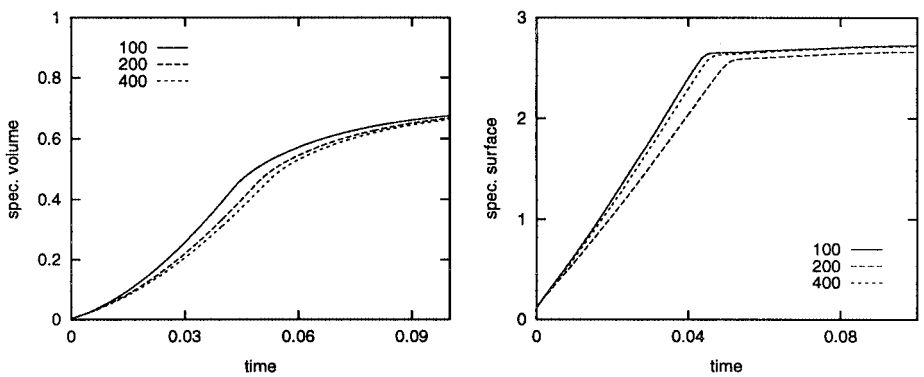

FIG. 14. Method of fully faceted interfaces. Evolution of specific volume and specific surface for different space discretizations.

numerical solution; and the prescribed finite number of admissible normal directions leads to a more stable algorithm.

5. EXAMPLES FOR THE TWO-SCALE METHOD

For the numerical realization of the two-scale model we consider the problem (25), (26) defined on a rectangular domain Ω of size $[0; 2] \times [0; 0.5]$ (c.f. Fig. 15), with material parameters $c_V = 1$, $K = 1$, $D = \varepsilon^2 \cdot D_0$ with $D_0 = 1$, $\lambda = 0.5$, $\sigma = \varepsilon\sigma_0$ with $\sigma_0 = 0.002$, initial temperature $T^{(0)} = 0$, and initial chemical potential $\mu_s^{(0)} = 0.5$. The function b is defined by $b(T, \mu) = LT - \lambda\mu$, and the latent heat L is specified below. The domain is cooled by the Neumann boundary condition $K \frac{\partial T}{\partial n} = -5$ on part of boundary Γ_4, while the remaining boundary is isolated. At initial time $t = 0$ small solid kernels are assumed to have just formed at the grid points of a uniform square grid with a density of $1/(4\varepsilon^2)$; this gives a local cell problem defined on a square with edge length 2. Let us recall that the two-scale model is an approximation for a whole family of phase transition problems depending on scale parameter ε with increasing accuracy for decreasing ε. The discretization of the macroscopic domain is done using a uniform rectangular grid with 8×3 elements. The problem is essentially one dimensional; in the graphs below we illustrate the properties of an array of eight crystals in x-direction.

For both problems, the discretization in time is done using an implicit Euler scheme and the space discretization using finite elements on a uniform rectangular grid using bilinear shape functions. Here, the local cell problems have to be solved for every node of the macroscopic grid. This is done with one of the two algorithms described above. The problems are coupled in a semiimplicit way. First, all the local cell problems are solved for the temperature of the previous time step; then the heat equation is solved with the new release of latent heat computed from the cell problems.

The results of the computation using the variational algorithm for the cell problems are depicted in Figs. 16–21. The cell problem is discretized with time step $\Delta t = 0.0001$ and a grid consisting of 400×400 elements, and the initial solid kernels are assumed to be disks of radius 0.05. In order to show the influence of macroscopic heat transport on the evolution of the solid crystals, we use two different values, $L = 10$ and $L = 5$, for the latent heat. Figure 16 shows the evolution of the first crystal (the one at the cooled boundary Γ_4) and the last crystal (the one at boundary part Γ_2) for latent heat $L = 10$. In Fig. 17 the evolution of the macroscopic specific volume and specific surface is depicted for crystals located at different distances from the cooled boundary. Crystal 0 is the one

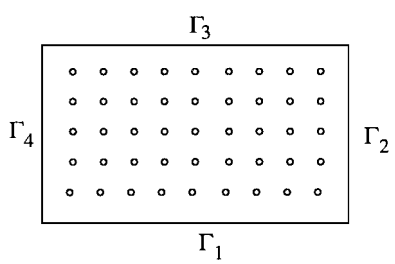

FIG. 15. Model problem for two-scale method.

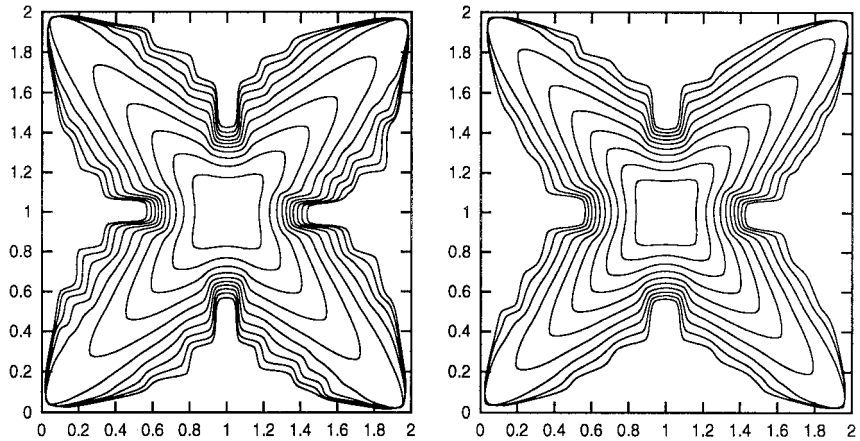

FIG. 16. Two-scale method with variational algorithm. Evolution of left and right crystal for latent heat $L = 10$.

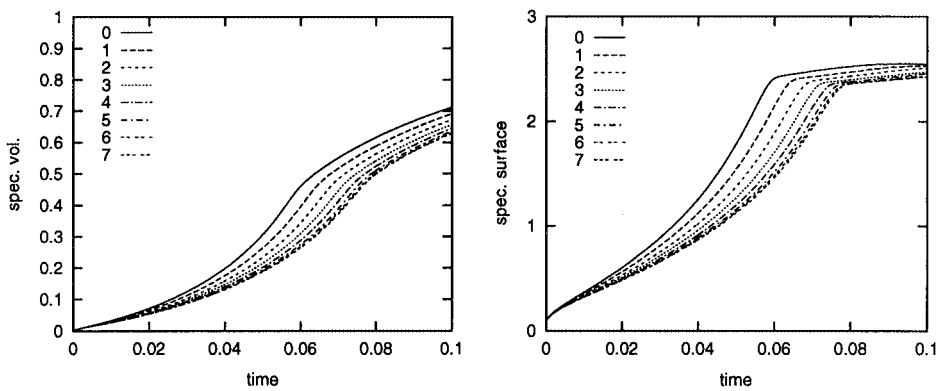

FIG. 17. Two-scale method with variational algorithm. Evolution of specific volume and specific surface for latent heat $L = 10$ and different crystals.

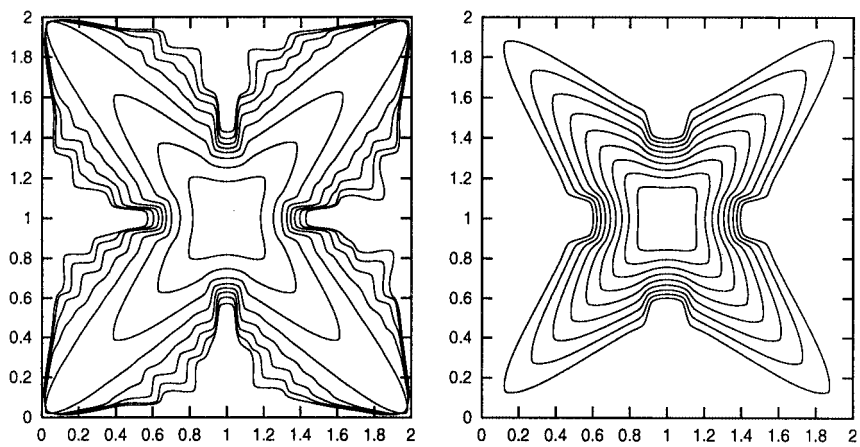

FIG. 18. Two-scale method with variational algorithm. Evolution of left and right crystal for latent heat $L = 5$.

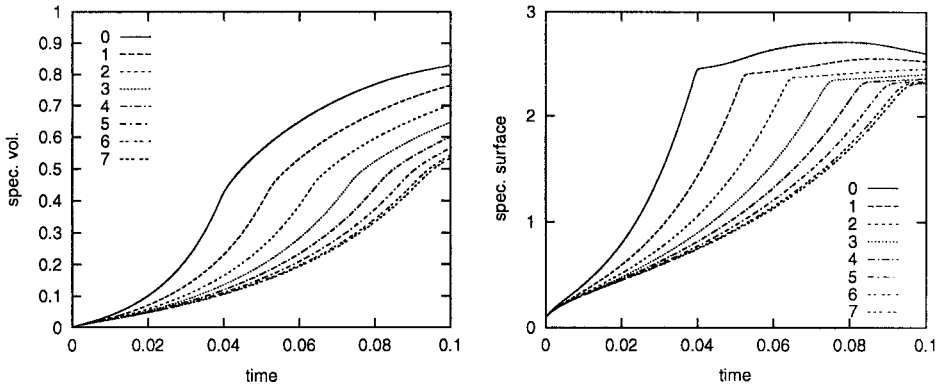

FIG. 19. Two-scale method with variational algorithm. Evolution of specific surface and specific volume for latent heat $L = 5$ and different crystals.

close to the cooled boundary, and crystal 7 is the one at the opposite side. Figure 18 and 19 show the corresponding graphs for latent heat $L = 5$. In this case, we observe a much bigger dependence of the microscopic data on the location of the crystal. The reason can be seen in the graph of the temperature distribution at a fixed time $t = 0.1$ in Fig. 21. For large value of the latent heat, the growth of the first crystal releases enough latent heat to almost compensate for the cooling condition on the boundary; this leads to an almost uniform temperature field, and the main driving force of the crystal growth is the initial solutal undercooling, which is essentially the same for all crystals. For small latent heat, the growth of the first crystals is limited by solute diffusion; hence they cannot release enough latent heat to consume all the boundary cooling, and the variation of the temperature field as well as that of the crystals is much bigger. Figure 20 depicts the shape of all eight computed crystals for latent heat $L = 5$ and time $t = 0.04$ in one picture.

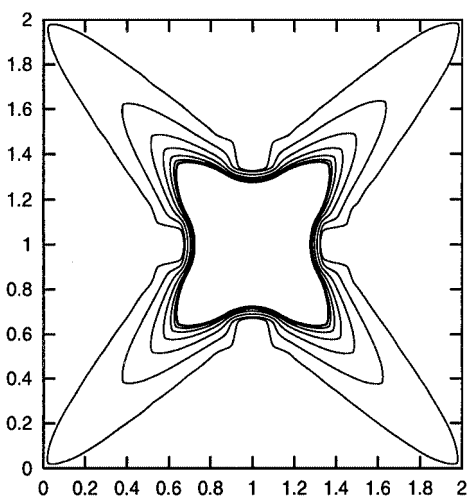

FIG. 20. Two-scale method with variational algorithm. Snapshot of all crystals for latent heat $L = 5$ at time $t = 0.04$.

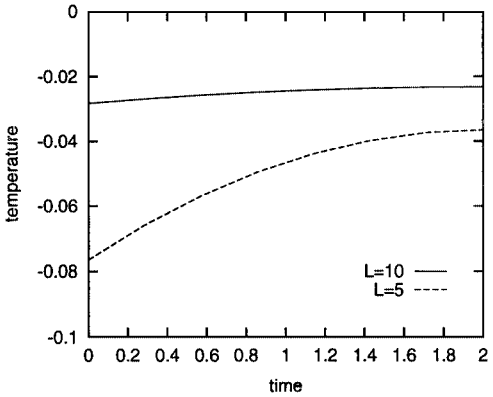

FIG. 21. Two-scale method with variational algorithm. Macroscopic temperature for latent heat $L = 10$ and $L = 5$ at time $t = 0.1$.

The same calculations have been done with the method of fully faceted interfaces for the solution of the local problems. Here, the problem is discretized using a grid of 200×200 elements, and the initial solid kernel is a square with edge length 0.05. Figures 22 and 23 show the evolution of the left and right crystals and the specific data for latent heat $L = 10$. In Figs. 24 and 25 the corresponding data are depicted for latent heat $L = 5$. Figure 26 shows the shape of the computed crystals for latent heat $L = 5$ and time $t = 0.04$ in one graph.

Unfortunately, according to the knowledge of the authors there are no experimental data or analytical results available to verify the computations. Comparing the results of both methods one observes that the shape of the crystals is slightly different. The crystals computed with the variational algorithm evolve a little faster than those computed with the method of fully faceted interfaces. This small difference is also seen in the macroscopic data, the specific volume, and specific surface, which are the important data for the two-scale model. The reason is the different physical models the algorithms are based on. While the variational method allows for a vanishing kinetic coefficient, this is not possible in the

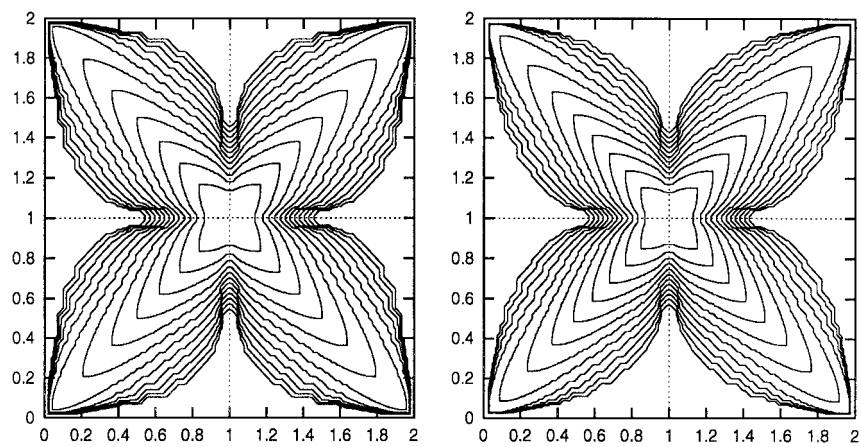

FIG. 22. Two-scale method with algorithm of fully faceted interfaces. Evolution of left and right crystal for latent heat $L = 10$.

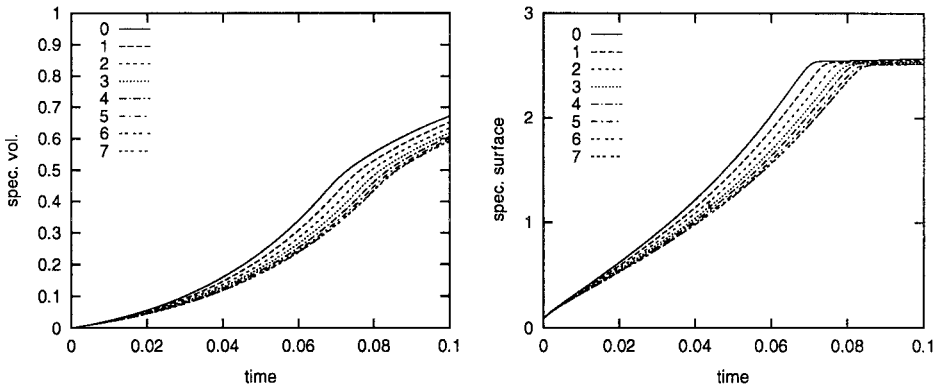

FIG. 23. Two-scale method with algorithm of fully faceted interfaces. Evolution of specific data for latent heat $L = 10$ and different crystals.

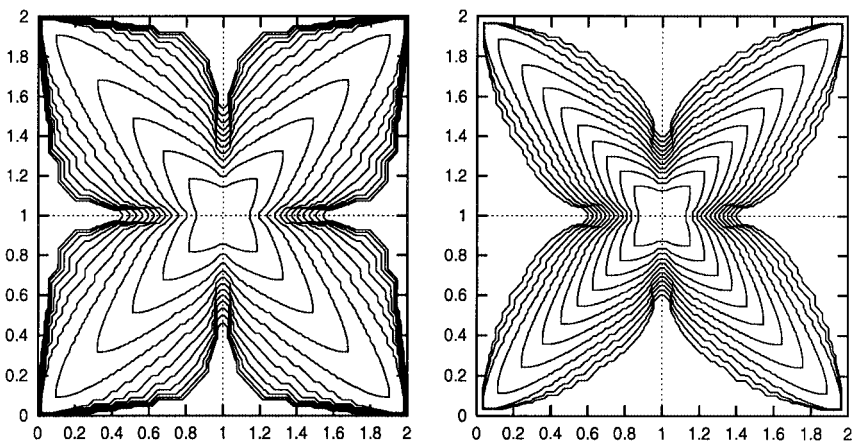

FIG. 24. Two-scale method with algorithm of fully faceted interfaces. Evolution of left and right crystal for latent heat $L = 5$.

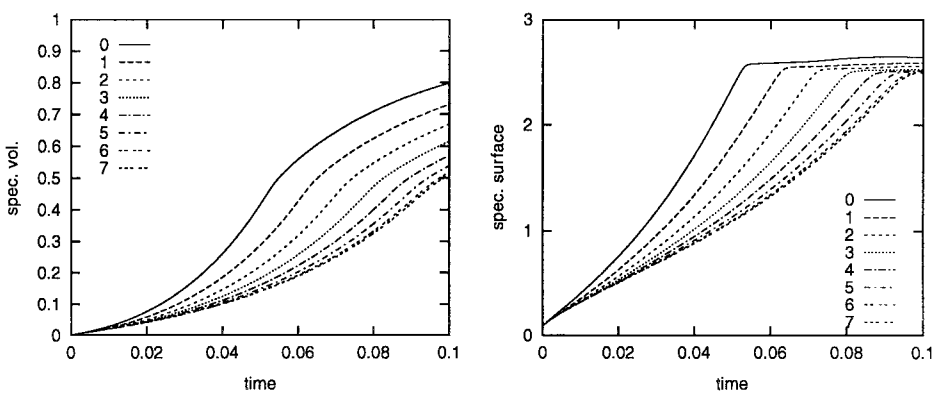

FIG. 25. Two-scale method with algorithm of fully faceted interfaces. Evolution of specific volume and specific surface for latent heat $L = 5$ and different crystals.

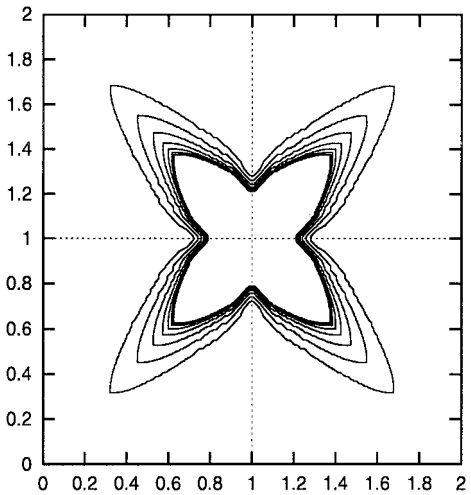

FIG. 26. Two-scale method with algorithm of fully faceted interfaces. Snapshot of all crystals for latent heat $L = 5$ at time $t = 0.04$.

method of fully faceted interfaces. Furthermore, the precise form of the anisotropy of the surface energy is different in the two algorithms.

6. CONCLUSIONS

We have presented a two-scale model for liquid–solid phase transitions in binary mixtures with an equiaxed dendritic microstructure neglecting convection. The model is derived with the method of formal asymptotic expansions; it is suitable for a small-scale microstructure and small solute diffusion. The periodicity assumptions required for a mathematically well-founded derivation of the model are, of course, physically unrealistic, but the model is perhaps also applicable for the nonperiodic situation, where only the macroscopic properties of the microstructure are of interest. A numerical discretization of the model is presented, based on two different methods for the computation of dendritic growth, and results of numerical computations are given. These results show that the method is in principle capable of describing macroscopic properties of the evolving microstructure at least phenomenologically. For a sufficiently small-scale microstructure the method is computationally cheaper than a direct simulation, because it requires the calculation of only a fixed number of crystals, independent of the scale of the microstructure (but dependent on the grid of the macroscopic problem). The method is very well suited for parallelization. However, it is still computationally expensive, because the quite challenging task of computation of crystal growth has to be carried out for every point of a macroscopic grid. In order to obtain a method capable of simulating physically realistic and technically important processes, some considerable further simplification is necessary. Such a simplification may be obtained by replacing the solution of the microscopic problems with a relation between the temperature field and a vector M of macroscopic properties of the evolving microstructure, containing, e.g., specific volume, specific surface, and possibly other quantities. Such relations may have the form of a direct functional relation $M(t, x) = \mathcal{M}(T(t, x), \dot{T}(t, x))$ or of an evolution equation $\dot{M}(t, x) = \mathcal{F}(T(t, x), M(t, x))$, with the latter example being more realistic. It is perhaps

possible to approximate such a relation by interpolation of the results of a few computations of our microscopic cell problem for different prescribed evolutions of the temperature. The thus-obtained constitutive law for the microstructure evolution may be employed to derive a completely macroscopic model. Such an approach can be also embedded in an adaptive procedure, where the evolution of a given crystal is computed by interpolation of previously computed data, if such data are available, and by the crystal growth algorithm, if such data are not available. This approach will not avoid the microscopic problems completely, but it may reduce the number of crystals to be computed considerably. In this sense, the results presented here can be considered as a first step toward a well-founded model suitable for technically interesting situations.

REFERENCES

1. F. Almgren and L. Wang, Mathematical existence of crystal growth with Gibbs–Thomson curvature effects, *J. Geom. Anal.* **10** (1), 1 (2000).
2. R. Almgren, Variational algorithms and pattern formation in dendritic solidification, *J. Comput. Phys.* **106**, 337 (1993).
3. C. Beckermann and C. Y. Wang, Multiphase/-scale modeling of alloy solidification, *Ann. Rev. Heat Transfer* **6**, 115 (1995).
4. G. Caginalp, An analysis of a phase field model of a free boundary, *Arch. Ration. Mech. Anal.* **92**, 205 (1986).
5. G. Caginalp and W. Xie, An analysis of phase field alloys and transition layers, *Arch. Rat. Mech. Anal.* **142**, 293 (1998).
6. X. Chen and F. Reitich, Local existence and uniqueness of solutions of the Stefan problem with surface tension and kinetic undercooling, *J. Math. Anal. Appl.* **164**, 350 (1992).
7. J. Escher, J. Prüss, and G. Simonett, *Analytical Solutions for a Stefan Problem with Gibbs–Thomson Correction*, Preprint No. 13/99 (Fachbereich Mathematik/Informatik, Universität Gesamthochschule Kassel, 1999).
8. M. E. Gurtin, *Thermomechanics of Evolving Phase Boundaries in the Plane* (Clarendon, Oxford 1993).
9. G. P. Ivantsov, Temperature field around spherical, cylindrical and needle-shaped crystals which grow in supercooled melt, *Dokl. Akad. Nauk USSR* **58**, 567 (1947) (in Russian).
10. D. Juric and G. Tryggvason, A front-tracking method for dendritic solidification, *J. Comput. Phys.* **123**, 127 (1996).
11. R. Kobayashi, A numerical approach to three-dimensional dendritic solidification, *Exp. Math.* **3** (1), 59 (1994).
12. R. Kobayashi, Modeling and numerical simulation of dendritic crystal growth, *Physica D* **63**, 410 (1993).
13. W. Kurz and D. J. Fisher, *Fundamentals of Solidification* (Trans Tech Publ., Aedermannsdorf, 1986).
14. S. Luckhaus, Solutions for the two-phase Stefan problem with the Gibbs–Thomson law for the melting temperature, *Eur. J. Appl. Math.* **1**, 101 (1990).
15. S. Luckhaus, *Solidification of Alloys and the Gibbs–Thomson Law*, Preprint (University of Bonn, 1994).
16. S. Luckhaus and A. Visintin, Phase transition in multicomponent system, *Manuscr. Math.* **43**, 261 (1983).
17. A. M. Meirmanov, *The Stefan Problem* (de Gruyter, Berlin, 1992).
18. I. Prigogine, *Thermodynamics of Irreversible Processes* (Interscience, New York, 1967).
19. E. V. Radkevich, On conditions for the existence of a classical solution of the modified Stefan problem (Gibbs–Thomson law), *Russ. Acad. Sci. Sb. Math.* **75** (1), 221 (1993).
20. M. Rappaz, Modelling of microstructure formation in solidification processes, *Int. Mater. Rev.* **34**(3), 93 (1989).
21. A. R. Roosen and J. E. Taylor, Modeling crystal growth in a diffusion field using fully faceted interfaces, *J. Comput. Phys.* **114**, 113 (1994).
22. A. Schmidt, Computation of three-dimensional dendrites with finite elements, *J. Comput. Phys.* **125**, 293 (1996).

23. M. C. Schneider and C. Beckermann, A numerical study of the combined effects of microsegregation, mushy zone permeability and flow, caused by volume contraction and thermosolutal convection, on macrosegregation and eutectic formation in binary alloy solidification, *Int. J. Heat Mass Transfer* **38** (18), 3455 (1995).
24. J. A. Sethian and J. Strain, Crystal growth and dendritic solidification, *J. Comput. Phys.* **98**, 231 (1992).
25. D. E. Tempkin, Growth rate of the needle-crystal formed in a supercooled melt, *Dokl. Akad. Nauk USSR* **132**, 609 (1960).
26. A. Visintin, Stefan problem with surface tension, in *Mathematical Models for Phase Change Problems*, edited by J. F. Rodrigues (Birkhäuser, Basel, 1989).
27. A. Visintin, *Models of Phase Transitions* (Birkhäuser, Boston, 1996).
28. J. Warren and W. J. Boettinger, The phase field method: simulation of dendritic alloy solidification during recalescence, *Metall. Mater. Trans. A* **27** (3), 657 (1996).
29. V. V. Zhikov, S. M. Kozlov, and O. A. Olejnik, *Homogenization of Differential Operators and Integral Functionals* (Springer-Verlag, Berlin, 1994).